Enhanced Ferromagnetism and Tunable Magnetism in Fe3GeTe2 Monolayer by Strain Engineering

Hu, X.; Zhao, Y.; Shen, X.; Krasheninnikov, A.; Chen, Z.; Sun, L.;

Originally published:

May 2020

ACS Applied Materials and Interfaces 12(2020), 26367-26373

DOI: https://doi.org/10.1021/acsami.0c05530

Enhanced Ferromagnetism and Tunable Magnetism in Fe_3GeTe_2 Monolayer by Strain Engineering

Xiaohui Hu,[*1,2] Yinghe Zhao,[3] Xiaodong Shen,[1,2] Arkady V. Krasheninnikov,[4,5] Zhongfang Chen,[*3] Litao Sun,[*6]

[1] College of Materials Science and Engineering, Nanjing Tech University, Nanjing 211816, China

[2] Jiangsu Collaborative Innovation Center for Advanced Inorganic Function Composites, Nanjing Tech University, Nanjing 211816, China

[3] Department of Chemistry, University of Puerto Rico, Rio Piedras Campus, San Juan, Puerto Rico 00931

[4] Institute of Ion Beam Physics and Materials Research, Helmholtz-Zentrum Dresden-Rossendorf, 01314 Dresden, Germany

[5] Department of Applied Physics, Aalto University School of Science, PO Box 11100, 00076 Aalto, Finland

[6] SEU-FEI Nano-Pico Center, Key Laboratory of MEMS of Ministry of Education, Collaborative Innovation Center for Micro/Nano Fabrication, Device and System, Southeast University, Nanjing 210096, China

Corresponding Author:

xiaohui.hu@njtech.edu.cn (XH); zhongfangchen@gmail.com (ZC); slt@seu.edu.cn (LS)

Abstract

Recent discovery of intrinsic ferromagnetism in Fe_3GeTe_2 (FGT) monolayer [*Nature* **2018**, *563*, 94; *Nat. Mater.* **2018**, *17*, 778] not only extended the family of 2D magnetic materials, but also stimulated further interest in the possibility to tune their magnetic properties without changing the chemical composition or introducing defects. By means of density functional theory computations, we explore strain effects on the magnetic properties of a FGT monolayer. We demonstrate that the ferromagnetism can be largely enhanced by the tensile strain in FGT monolayer due to the competing effects of direct exchange and superexchange interaction. The average magnetic moments of Fe atoms increase monotonically with increasing biaxial strain from -5% to 5% in FGT monolayer. The changes in magnetic moments with strain in FGT monolayer are related to the charge transfer induced by the changes in the bond lengths. Given the successful fabrication of FGT monolayer, the strain-tunable ferromagnetism in FGT monolayer can stimulate the experimental effort in this field. This work also suggests an effective way to control magnetic properties of FGT monolayer. The pronounced magnetic response towards the biaxial strain can be used to design the magneto-mechanical coupling spintronic devices based on FGT.

Introduction

Two-dimensional (2D) materials, such as graphene, boron nitride, ternary boron-carbon-nitrogen systems, and transition metal dichalcogenides, have demonstrated their great potentials in nanoelectronics due to their fascinating properties [1-4]. However, these materials are non-magnetic, which limits their use in spintronic devices.

Encouragingly, first-principles calculations indicated that magnetism can be induced in these systems by defects and/or impurities [5-10]. Thus, significant efforts have been made to introduce magnetism through defect engineering, e.g., by cutting graphene to ribbons [11], introducing transition metal atoms [12, 13], creating vacancy defects [14, 15] in these 2D materials. Unfortunately, although localized magnetic moments can be created using these methods, it is difficult to introduce long-range ferromagnetic ordering in these non-magnetic 2D materials.

The very recently experimentally realized 2D materials with intrinsic ferromagnetic ordering can help overcome all these limitations, which has great potentials for new spintronics applications [16-19]. It has been experimentally demonstrated that monolayer CrI_3 is an Ising ferromagnet with out-of-plane spin orientation and the Curie temperature of 45K [20]. A recent study has shown that ferromagnetic order is present in the ultrathin layered material $Cr_2Ge_2Te_6$ at low temperatures [21]. The magnetism in bilayer CrI_3 and few-layered $Cr_2Ge_2Te_6$ can be further controlled by electric field [22-24]. In addition to CrI_3 and $Cr_2Ge_2Te_6$, other novel 2D ferromagnets have been proposed [25-27]. Among these 2D ferromagnetic materials, Fe_3GeTe_2 (FGT) is particularly promising [28-30], as ferromagnetism persists in FGT down to the monolayer, and the ferromagnetic transition temperature of FGT monolayer is 130K, higher than that of other 2D ferromagnetic materials [28, 30]. Although 2D ferromagnetic order has been found experimentally in FGT monolayer, the use of this system in actual applications requires the ability to tune its magnetic properties and enhance the stability of the ferromagnetic state. Thus, achieving a precise control over

magnetic moments and ferromagnetic stability through external parameters is highly desirable for the practical applications of this material in spintronics.

Strain engineering, sometimes referred to as “straintronics” [31], is a promising route to modulate the electronic and magnetic properties of 2D materials [32-39]. It has been demonstrated that graphene can be tuned from metallic to insulating system by applying strain along different crystallographic directions [32, 33]. The optical band gap of MoS_2 membranes can be continuously tuned by applying biaxial strain [34]. It was predicted that tensile strain along the zigzag direction can greatly enhance ferromagnetic stability of graphene with a topological line defect, while tensile strain along the armchair direction quickly reduces magnetic moments [36]. The half-fluorinated BN and GaN layers exhibit an interesting magnetic transition from antiferromagnetism to ferromagnetism by applying strain, and a half-metallic behavior can be achieved at the 6% compression [37]. Likewise, ferromagnetism was predicted in layered NbS_2 and $NbSe_2$ under biaxial tensile strain [38]. The induced magnetic moments can also be obviously enhanced by the tensile strain. In VX_2 monolayers (X=S, Se), the magnetic coupling and magnetic moments were predicted to increase rapidly with increasing strain, which arises from the strong ionic-covalent bonds [39]. These results strongly indicate that a systematical study of strain effect on magnetic behavior of FGT monolayer is highly desirable.

In this work, by means of density functional theory (DFT) calculations, we explore strain effects on the magnetic properties of a FGT monolayer. We show that the tensile strain can considerably enhance the ferromagnetism of the monolayer. The strain-

tunable ferromagnetism in FGT monolayer predicted in our simulations can stimulate the experimental effort in this field. In addition, the average magnetic moments of Fe atoms increase monotonically with increasing strain from -5% to 5% in FGT monolayer. The result suggests that strain engineering is an effective route to enhance the tunability of magnetic properties in FGT monolayer.

Computational Method

Our DFT calculations were performed using the VASP package [40, 41] within the projector-augmented-wave (PAW) method [42, 43]. Spin-polarized local density approximation (LDA) [44] was used as the exchange-correlation functional. The previous studies [30, 45] demonstrated that LDA+U, PBE and PBE+U functionals overestimate magnetic moments for bulk FGT and FGT monolayer, whereas LDA can accurately describe the FGT system [46-48]. Hence, the LDA functional was chosen in our work. The energy cutoff of the plane wave basis set was 600 eV. The structures were relaxed until the energy and the force on each atom were less than 10^{-5} eV and 0.005 eV/ Å, respectively. The k-point sampling of 29 × 29 × 1 was used for unit cell of FGT monolayer, and a 10 × 20 × 1 k-point mesh was used for the 2 × 1 × 1 supercell. A vacuum spacing of 16 Å was introduced to avoid the spurious interactions between the periodic images of the system.

Results and discussion

FGT monolayer has been successfully fabricated by Xu's [28] and Zhang's groups [30]. FGT monolayer is composed of five atomic layers: the top and bottom sublayers are Te atoms, the second and fourth sublayers are Fe1 and Fe2 atoms, the middle

sublayer is made up of Fe3 and Ge atoms (Figure 1(a)). There are two inequivalent Fe sites in FGT monolayer, where Fe1 and Fe2 atoms are located at the equivalent sites, while Fe3 atom has the inequivalent site. Our DFT calculation showed that the lattice parameter of FGT monolayer is 3.91Å, which is in a good agreement with the previous results [30, 45, 49]. The bond lengths and the bond angles are presented in Table S1 of the Supporting Information. Spin-density distribution in FGT monolayer (Figure S1, Supporting Information) indicates that the magnetic moments dominantly localize on Fe atoms, and the average local magnetic moment of Fe atoms is 1.53μ_B, which agrees with the previous studies [30, 45, 49]. The spin-polarized band structure of FGT monolayer (Figure 1(b)) exhibits metallic behavior for the spin-up and spin-down channels, similar to its bulk. The partial density of states (PDOS) analysis (Figure S2, Supporting Information) indicates that the Fe *d* orbitals mainly contribute to the metallicity.

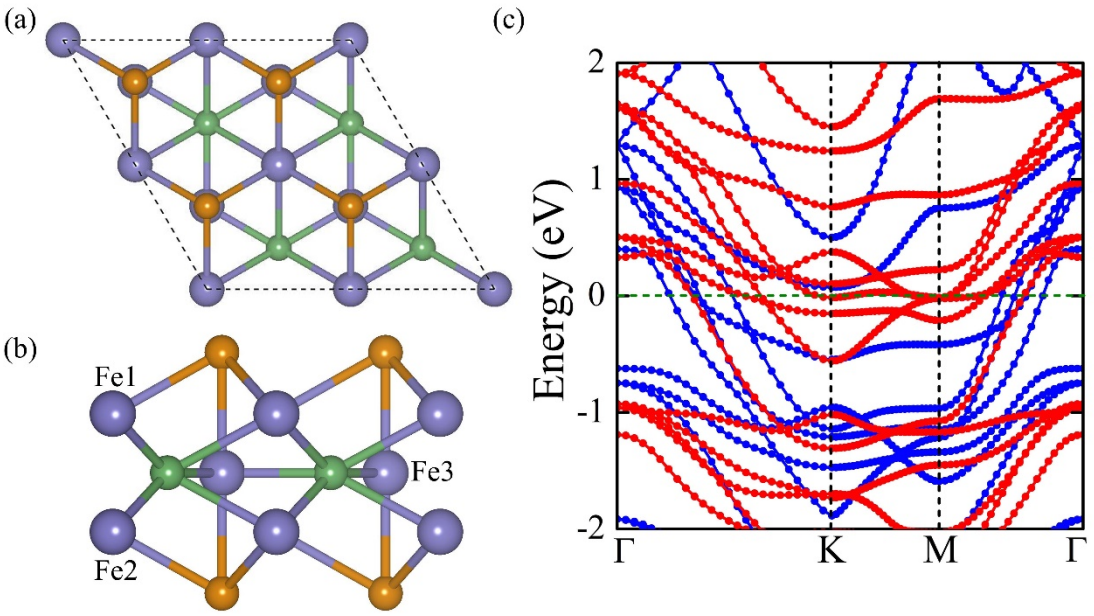

Figure 1. (a) Top and (b) side views of the structural models of FGT monolayer. The purple, green, and yellow balls stand for Fe, Ge, and Te atoms, respectively. Fe sites

are numbered by Fe1, Fe2 and Fe3, respectively, where Fe1 and Fe2 atoms are located at two equivalent sites, while Fe3 atom has the inequivalent site. (c) Spin-polarized band structures of FGT monolayer. The blue and red dot lines denote spin-up and spin-down channels, respectively. The Fermi level is set at zero, denoted by the olive dashed line.

FGT monolayer is known to have the ferromagnetic (FM) coupling of magnetic moments localized on Fe atoms, and the FM ordered spin is more desirable in practical applications in spintronic devices. However, it is not clear how the strain influences the FM spin ordering of FGT monolayer. Therefore, we studied strain effects on the stability of ferromagnetism in FGT monolayer. The strain effects were modeled by applying the in-plane biaxial strain along the lattice vectors. The biaxial strain is defined as $\varepsilon = \Delta c/c_0$, where c_0 and $c = c_0 \pm \Delta c$ are the unstrained and strained lattice constants of FGT monolayer, respectively. To examine the stability of FGT monolayer under the tensile and compressive strain, we perform the phonon spectrum calculation of FGT monolayer at -5%, -3%, 0% and 3%, 5% strain, respectively. It can be seen from Figure S3(a)-(d) that FGT monolayer is dynamically stable at -3%, 0%, 3%, 5% strain. However, it is evident from Figure S3(e) that FGT monolayer is unstable at -5% compressive strain. It can thus be concluded that FGT monolayer is dynamically stable under the tensile strain and moderate compressive strain, while it is unstable at large compressive strain. We note, though that experimentally, strain engineering of 2D materials is done by transferring the 2D material on a flexible substrate [50] an making useof lattice constant or thermal-expansion mismatch. The substrate can then increase

the stability of FGT monolayer. Therefore, following the previous theoretical studies [37, 39], we explore the stability of ferromagnetism in FGT monolayer with strain from -5% (compressive) to 5% (tensile).

To investigate the magnetic couplings between the magnetic moments localized on Fe atoms, we examine the spin configurations for FGT monolayer using a 2×1×1 supercell. According to the spin ordering of Fe atoms, the four typical magnetic structures were considered, which are depicted in Figure 2(a): (i) the ferromagnetic state, with FM spin ordering at each Fe atoms, denoted by FM; (ii) the antiferromagnetic state, with FM spin ordering at Fe1 and Fe2 atoms, the antiferromagnetically (AFM) spin ordering with Fe3 atom in the same cell, but with opposite ordering in the different cell, denoted by AFM1; (iii) the antiferromagnetic state, with FM ordered spins at Fe1, Fe2 and Fe3 atoms in the same cell, but with opposite ordering in the different cell, denoted by AFM2; (iv) the antiferromagnetic state, with FM spin ordering at Fe1 and Fe3 atoms, AFM spin ordering with Fe2 atom in the same cell, but with opposite ordering in the different cell, denoted by AFM3. Figure 2 (b) display the spin density distribution of the four magnetic structures. Note that AFM2 configuration in FGT monolayer is not stable, and it will transfer to the AFM1 coupling after geometry optimization (see Figure 2(b)). The FM coupling is the lowest energy state, which is more stable than AFM1 and AFM3 configurations by an energy difference of 106 and 97 meV, respectively. We also construct other possible AFM configurations, such as AFM4, AFM5, AFM6, AFM7 (Figure S4, Supporting

Information). It is found that these AFM configurations in FGT monolayer are not stable.

The energy difference $\Delta E = E_{AFM3} - E_{FM}$ at various strain values is presented in Figure 2(c). Here E_{AFM3} and E_{FM} are the total energies of AFM3 and FM configurations, respectively. It is found that the energy difference exhibits a significant increase with increasing strain from -5% to 5% for FGT monolayer. As the tensile strain increases, the energy difference rapidly increases and reaches 451 meV at 5% strain, nearly 5-fold higher than in the unstrained FGT. At the same time, the FM stability of FGT monolayer is remarkably enhanced, as evidenced by the increased energy difference with tensile strain. But for the compressive strain on FGT, the energy difference decreases with higher compression, and the FM coupling is weakened. This indicates that the tensile strain can significantly enhance the FM stability of FGT monolayer.

In order to understand if the FM coupling could be experimentally implemented, we considered possible structural instabilities in the considered range of strain. Figure 2(d) exhibits the variation of strain energy with applied strain: the strain energy is a quadratic function of strain. This indicates that the FM coupling holds in the elastic range, which has potential applications in electromechanical nanodevices.

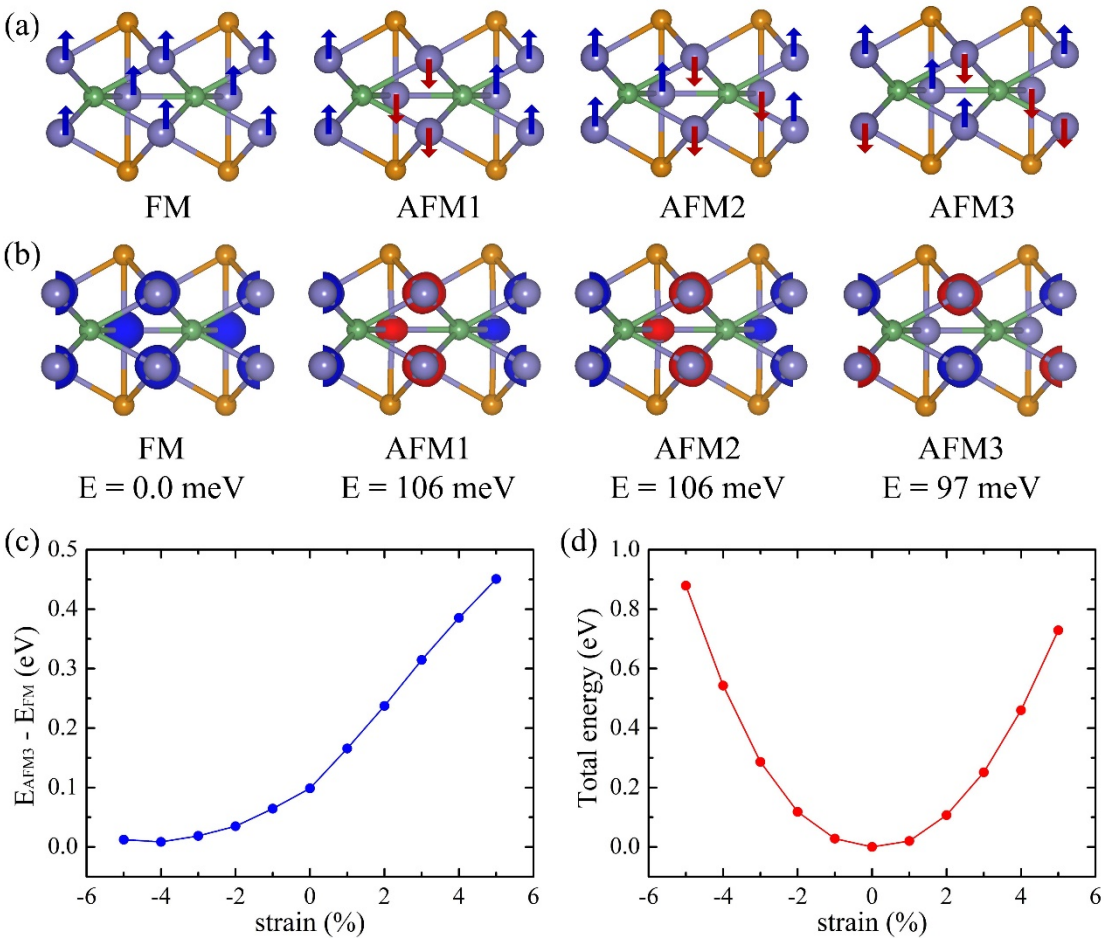

Figure 2. (a) Four different magnetic configurations and (b) spin-density distribution in FGT monolayer, depicted as FM, AFM1, AFM2 and AFM3. (c) The energy difference between AFM3 and FM coupling and (d) the total energy as a function of applied strain in FGT monolayer.

The stability of FM coupling can be understood using the Goodenough-Kanamori-Anderson (GKA) rules [51-53]. The magnetic ground state of FGT monolayer is governed by the direct exchange interaction and the superexchange interaction. For the direct exchange interaction, the *d* orbitals on the nearest-neighbor Fe atoms overlap directly, without a mediation atom. Thus, it gives rise to AFM coupling, and it is governed by the distance between the neighboring Fe atoms. On the other hand, for the

super-exchange interaction, the *d* orbitals on the nearest-neighbor Fe atoms overlap with the *p* orbitals of Ge or Te atoms. Consequently, the superexchange mediated by Ge or Te atoms gives rise to FM coupling. The FM coupling strength is mainly sensitive to the Fe-Te (Ge)-Fe angle. If superexchange interaction is stronger than direct exchange interaction, FGT exhibits FM coupling, otherwise it is in AFM coupling.

The three different paths for superexchange interaction between the nearest-neighbor Fe atoms in FGT monolayer are shown in Figure 3(a). Figure 3(b) and 3(c) give the dependence of the distance and the Fe-Te (Ge)-Fe angle on strain. As the strain increases, the distances of Fe1-Fe1 (d1) and Fe1-Fe3 (d2) increase, while the Fe1-Fe2 (d3) decreases. The angle of Fe1-Te-Fe1 (θ1) and Fe1-Te-Fe3 (θ2) increase, whereas the angle of Fe1-Ge-Fe2 (θ3) decreases as the strain increases. The delicate balance and competing nature of the direct exchange and superexchange interaction under the applied strain result in the stability of FM coupling. In addition, as Fe atoms have a nearly filled *d*-shell, there is a relatively small spatial hybridization between Fe atoms, but a strong Fe-Te (Ge) covalent interaction, which leads to the direct exchange interaction being smaller than the superexchange interaction, and thus the AFM direct exchange is weakened, and the FM coupling becomes more stable than the AFM coupling.

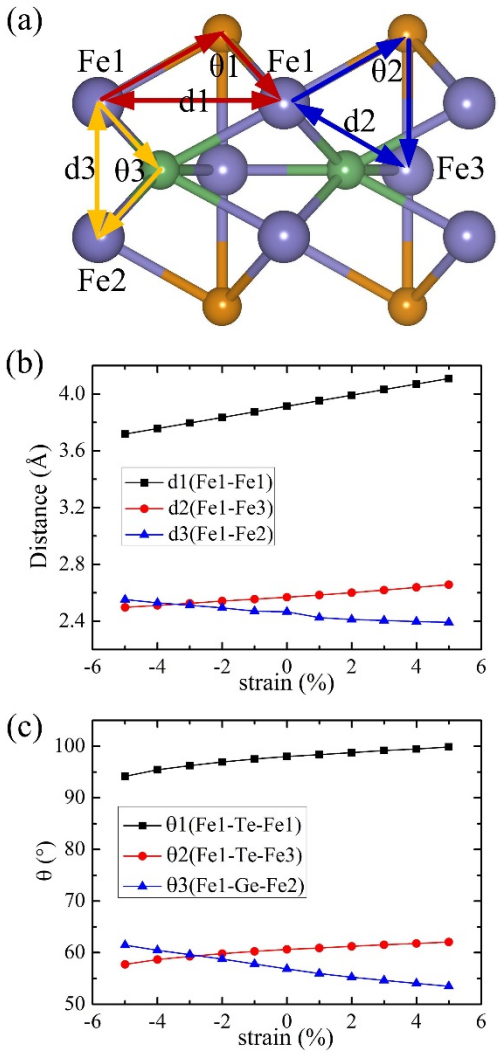

Figure 3. (a) Three different paths for superexchange interaction between the nearest-neighbor Fe atoms in FGT monolayer. Fe1-Te-Fe1, Fe1-Te-Fe3 and Fe1-Ge-Fe2 paths are represented by the red, blue and yellow solid line triangles, respectively. Strain dependence of (b) the distance and (c) the Fe-Te (Ge)-Fe angle (Fe1-Fe1 distance, d1; Fe1-Fe3 distance, d2; Fe1-Fe2 distance, d3; Fe1-Te-Fe1 angle, θ1; Fe1-Te-Fe3 angle, θ2; Fe1-Ge-Fe2 angle, θ3).

To gain further insights into the magnetic properties of FGT monolayer with applied strain, we examined the spin-density distributions (Figure 4(a)). Evidently, external

strain has a significant effect on the magnetic properties of FGT monolayer. We further examined the strain dependence of the magnetic moments of atoms (Figures 4(b) and 4(c)). For simplified, the magnetic moments of Fe1 and Fe3 atoms in FGT monolayer are named as M_{Fe1} and M_{Fe3}, and that of Ge and Te atoms are named as M_{Ge} and M_{Te}, respectively. We found that the M_{Fe1} increases monotonically with strain increasing from -5% to 5% in FGT monolayer. Under tensile strain, the M_{Fe1} reach 2.26 μ_B at ε = 5%, approximately 126% increment compared to the case of undeformed FGT monolayer. For the compressive strain, the M_{Fe1} decreases down to 1.46 μ_B at ε = -5%. Different from the case of M_{Fe1}, the M_{Fe3} first decreases, then increases slightly with the strain from -5% to 5%. The M_{Fe3} is calculated to be 1.33 μ_B, 1.02μ_B, 1.11 μ_B at ε = -5%, 0, 5%, respectively. Although the distinct change of M_{Fe1} and M_{Fe3}, the average magnetic moment of Fe atoms increases monotonically with increasing strain from -5% to 5% in FGT monolayer. On the other hand, the M_{Ge} (M_{Te}) also increases with the strain from 0.039 μ_B (0.019 μ_B) at -5% to 0.071 μ_B (0.028 μ_B) at 5%. The results suggest that the Fe atoms mainly contribute the spin polarizations, while the Ge and Te atoms have little contribution to the magnetism. The spin polarizations in FGT monolayer is robust for wide range of strain. As mentioned above, the structural breakage will not occur in a large elastic range. Therefore, the large elastic range will provide the possibility to modulate the spin state and the magnetic properties by applying tensile or compressive strains.

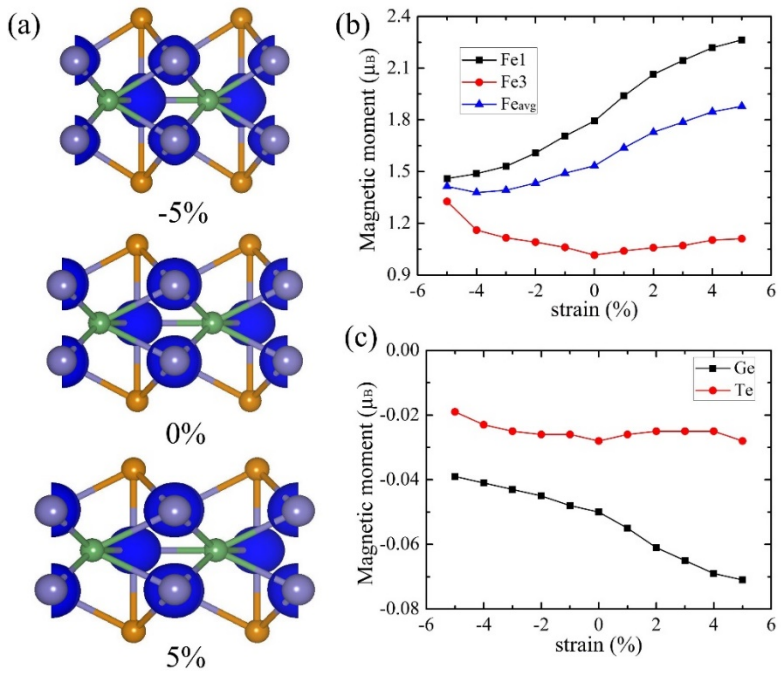

Figure 4. (a) Spin-density distribution of FGT monolayer with -5%, 0, 5% strain. The isovalues are 0.02 e/Å^3. Strain dependence of magnetic moment (b) per Fe1 and Fe3 atoms, and (c) per Ge and Te atoms in FGT monolayer.

The changes in the magnetic moments with strain can be understood by examining the bond lengths, the charge transfer, and the PDOS of FGT monolayer under -5%, 0, 5% strain. The geometric details of FGT monolayer under biaxial strain are presented in Figure 5 (a). Due to the Poisson effect, stretching of in-plane biaxial direction will result in contraction in the perpendicular direction. Thus, upon applying biaxial strain on FGT monolayer, the distance of Fe1-Fe2 and the bond length of Fe3-Te (denoted as $d_{Fe1\text{-}Fe2}$ and $d_{Fe3\text{-}Te}$) becomes reduced in the perpendicular direction, whereas the bond lengths of Fe1-Te and Fe3-Ge (denoted as $d_{Fe1\text{-}Te}$ and $d_{Fe3\text{-}Ge}$) increase in the plane direction. We note that the bond lengths $d_{Fe1\text{-}Te}$ and $d_{Fe3\text{-}Ge}$ increase by 5.75% and 10.53% for FGT monolayer at a 5% tensile strain as compared to that at a -5% compressive

strain. Due to the change of bond length, the obvious charge transfer in FGT monolayer was found (Figure 5(b)). Each Fe1 (Te) atom loses (gains) about 0.08 (0.08), 0.14 (0.11) and 0.21 (0.19) electron charge at -5%, 0 and 5% strain, respectively. On the other hand, each Fe3 (Ge) atom gains (loses) about 0.25 (0.19), 0.13 (0.06) and 0.16 (0.07) electron charge at -5%, 0 and 5% strain, respectively. The charge transfer between Fe1 and Te (Fe3 and Ge) atoms has the completely opposite trend, implying the charge transfer mainly happens between Fe1 and Te (Fe3 and Ge) atoms. Furthermore, we found that the amount of charge transferred from Fe1 atom increases monotonically, whereas that of Fe3 atom first decreases, then increases slightly with the increase of strain from -5% to 5%, which has the similar trend with the magnetic moment change of Fe1 (Fe3) atoms with strain (Figure 4(b)). Due to the charge transfer, it can be also seen from Figure 5(c) that the spin splitting of Fe1 3*d* orbital near the Fermi level becomes larger with increasing strain from -5% to 5%, as evident from the enhanced spin splitting of the a and b states in PDOS (Figure 5 (c)), which gives rise to an increase in the magnetic moments of Fe1 atoms with strain. At the same time, for Fe3 atoms the spin polarization is increased at -5% compressive strain and 5% tensile strain as compared to the unstrained FGT monolayer (Figure 5(d)), which results in the increase in the magnetic moment of Fe3 atoms with increasing compressive and tensile strains, respectively. Therefore, the charge transfer between Fe1 and Te (Fe3 and Ge) atoms can be viewed as an important mechanism for the variation in the magnetic moment of FGT monolayer with strain.

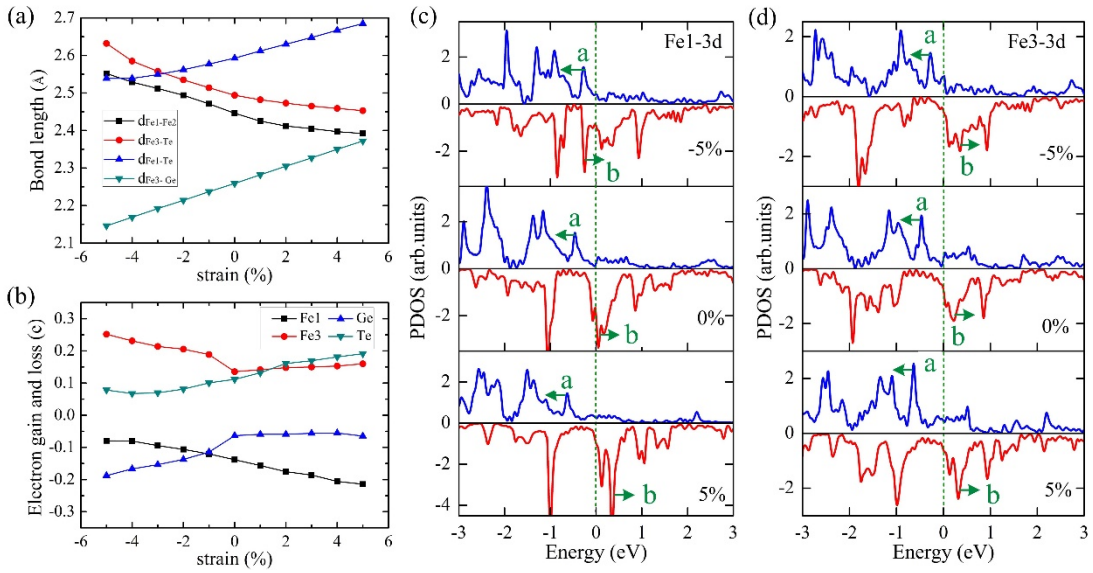

Figure 5. Strain dependence of (a) the distance and the bonding length (Fe1-Fe2 distance, $d_{Fe1-Fe2}$; Fe3-Te bond length, d_{Fe3-Te}; Fe1-Te bond length, d_{Fe1-Te}; Fe3-Ge bond length, d_{Fe3-Ge}). (b) the electron transfer of Fe, Ge and Te atoms in FGT monolayer. PDOS of (c) Fe1 atom and (d) Fe3 atom in FGT monolayer under -5%, 0% and 5% biaxial strain, respectively. The blue and red solid lines indicate spin-up and spin-down channels. The Fermi level is indicated by the olive dashed lines.

Conclusion

In summary, spin-polarized DFT calculations have been performed to investigate the magnetic properties of FGT monolayer under biaxial strain. We show that the stability of ferromagnetism can be largely enhanced by the tensile strain in FGT monolayer due to the competing effects of direct exchange and superexchange interactions. The magnetic moments of Fe1 atoms increase monotonically with increasing strain in FGT monolayer, whereas the magnetic moments of Fe3 atoms first decrease, then increase slightly with strain changing from -5% to 5%. A detailed analysis revealed that the observed variation in the magnetic moment of FGT monolayer arises from the charge

transfer induced by the changes in bond lengths under strain. Given the successful fabrication and observation of intrinsic ferromagnetism in FGT monolayer, we strongly believe that this study will stimulate the experimental effort in this field, and the strain engineering can serve as an effective way to control magnetic properties of FGT monolayer, which can greatly facilitate the development of spintronic devices based on 2D materials. The pronounced magnetic response towards biaxial strain in FGT monolayers can also greatly facilitate the development of the magneto-mechanical coupling spintronic devices.

Acknowledgements

This work is supported in China by the National Natural Science Foundation of China (No.11604047), the Natural Science Foundation of Jiangsu Province (No. BK20160694), Jiangsu Planned Projects for Postdoctoral Research Funds (No. 2019K010A), the Priority Academic Program Development of Jiangsu Higher Education Institutions (PAPD), the Fundamental Research Funds for the Central Universities, and the open research fund of Key Laboratory of MEMS of Ministry of Education, Southeast University, and in USA by NSF-CREST Center for Innovation, Research and Education in Environmental Nanotechnology (CIRE2N) (Grant Number HRD-1736093). AVK acknowledges funding from the German Research Foundation (DFG), project KR 48661/2. We are thankful for the computational resources from the High Performance Computing Center of Nanjing Tech University, National Supercomputer Center in Tianjin and CSC Finland.

References

[1] Castro Neto, A. H.; Guinea, F.; Peres, N. M. R.; Novoselov, K. S.; Geim, A. K. The Electronic Properties of Graphene. Rev. Mod. Phys. 2009, 81, 109−162.

[2] Hu, X.; Bjorkman, T.; Lipsanen, H.; Sun, L.; Krasheninnikov, A. V. Solubility of Boron, Carbon, and Nitrogen in Transition Metals: Getting Insight into Trends from First-Principles Calculations. J. Phys. Chem. Lett. 2015, 6, 3263–3268.

[3] Duan, X.; Wang, C.; Pan, A. Yu. R.; Duan, X. Two-Dimensional Transition Metal Dichalcogenides as Atomically Thin Semiconductors: Opportunities and Challenges. Chem. Soc. Rev. 2015, 44, 8859–8876.

[4] Hu, X.; Wang, Y.; Shen, X.; Krasheninnikov, A. V.; Sun, L.; Chen, Z. 1T Phase as an Efficient Hole Injection Layer to TMDs Transistors: A Universal Approach to Achieve P-type Contacts. 2D Mater. 2018, 5, 031012.

[5] Yazyev, O. V.; Helm, L. Defect-Induced Magnetism in Graphene. Phys. Rev. B 2007, 75, 125408.

[6] Santos, E. J. G.; Sánchez-Portal, D.; Ayuela, A. Magnetism of Substitutional Co Impurities in Graphene: Realization of Single π Vacancies. Phys. Rev. B 2010, 81, 125433.

[7] Krasheninnikov, A. V.; Lehtinen, P. O.; Foster, A. S.; Pyykko, P.; Nieminen, R. M. Embedding Transition-Metal Atoms in Graphene: Structure, Bonding, and Magnetism. Phys. Rev. Lett. 2009, 102, 126807.

[8] Hu, X.; Zhang, W.; Sun, L.; Krasheninnikov, A. V. Gold-Embedded Zigzag Graphene Nanoribbons as Spin Gapless Semiconductors. Phys. Rev. B 2012, 86, 195418.

[9] Hu, X.; Wan, N.; Sun, L.; Krasheninnikov, A. V. Semiconductor to Metal to Half-Metal Transition in Pt-Embedded Zigzag Graphene Nanoribbons. J. Phys. Chem. C 2014, 118, 16133–16139.

[10] Karthikeyan, J.; Komsa, H.; Batzill, M.; Krasheninnikov, A. V. Which Transition Metal Atoms can be Embedded into Two-Dimensional Molybdenum Dichalcogenides and Add Magnetism? Nano Lett. 2019, 19, 4581–4587.

[11] Magda, G. Z.; Jin, X.; Hagymási, I.; Vancsó, P.; Osváth, Z.; Nemes-Incze, P.; Hwang, C.; Biró, L. P.; Tapasztó, L. Room-Temperature Magnetic Order on Zigzag Edges of Narrow Graphene Nanoribbons. Nature 2014, 514, 608–611.

[12] Lin, Y.; Teng, P.; Chiu, P.; Suenaga, K. Exploring the Single Atom Spin State by Electron Spectroscopy. Phys. Rev. Lett. 2015, 115, 206803.

[13] Coelho, P. M.; Komsa, H. P.; Lasek, K.; Kalappattil, V.; Karthikeyan, J.; Phan, M. H.; Krasheninnikov, A. V.; Batzill, M. Room Temperature Ferromagnetism in $MoTe_2$ by Post-Growth Incorporation of Vanadium Impurities. Adv. El. Mater. 2019, 5, 1900044.

[14] Wang, S.; Robertson, A.; Warner, J. H. Atomic Structure of Defects and Dopants in 2D Layered Transition Metal Dichalcogenides. Chem. Soc. Rev. 2018, 47, 6764−6794.

[15] Cai, L.; He, J.; Liu, Q.; Yao, T.; Chen, L.; Yan, W.; Hu, F.; Jiang, Y.; Zhao, Y.; Hu, T.; Sun, Z.; Wei, S. Vacancy-Induced Ferromagnetism of MoS_2 Nanosheets. J. Am. Chem. Soc. 2015, 137, 2622–2627.

[16] Burch, K. S.; Mandrus, D.; Park, J. G. Magnetism in Two-Dimensional van der

Waals Materials. Nature 2018, 563, 47.

[17] Gong, C.; Zhang, X. Two-Dimensional Magnetic Crystals and Emergent Heterostructure Devices. Science 2019, 363, 706.

[18] Cortie, D. L.; Causer, G. L.; Rule, K. C.; Fritzsche, H.; Kreuzpaintner, W.; Klose, F. Two-Dimensional Magnets: Forgotten History and Recent Progress towards Spintronic Applications. Adv. Funct. Mater. 2019, 1901414.

[19] Li, H.; Ruan, S.; Zeng, Y. J. Intrinsic van der Waals Magnetic Materials from Bulk to the 2D Limit: New Frontiers of Spintronics. Adv. Mater. 2019, 31, 1900065.

[20] Huang, B.; Clark, G.; Navarro-Moratalla, E.; Klein, D. R.; Cheng, R.; Seyler, K. L.; Zhong, D.; Schmidgall, E.; McGuire, M. A.; Cobden, D. H.; Yao, W.; Xiao, D.; Jarillo-Herrero, P.; Xu, X. Layer-Dependent Ferromagnetism in a van der Waals Crystal Down to the Monolayer Limit. Nature 2017, 546, 270–273.

[21] Gong, C.; Li, L.; Li, Z.; Ji, H.; Stern, A.; Xia, Y.; Cao, T.; Bao, W.; Wang, C.; Wang, Y.; Qiu, Z. Q.; Cava, R. J.; Louie, S. G.; Xia, J.; Zhang, X. Discovery of Intrinsic Ferromagnetism in Two-Dimensional van der Waals Crystals. Nature 2017, 546, 265–269.

[22] Jiang, S.; Li, L.; Wang, Z.; Mak, K. F.; Shan, J. Controlling Magnetism in 2D CrI_3 by Electrostatic Doping. Nat. Nanotechnol. 2018, 13, 549–553.

[23] Huang, B.; Clark, G.; Klein, D. R.; MacNeill, D.; Navarro-Moratalla, E.; Seyler, K. L.; Wilson, N.; McGuire, M. A.; Cobden, D. H.; Xiao, D.; Yao, W.; Jarillo-Herrero, P.; Xu, X. Electrical Control of 2D Magnetism in Bilayer CrI_3. Nat. Nanotechnol. 2018, 13, 544–548.

[24] Wang, Z.; Zhang, T.; Ding, M.; Dong, B.; Li, Y.; Chen, M.; Li, X.; Huang, J.; Wang, H.; Zhao, X.; Li, Y.; Li, D.; Jia, C.; Sun, L.; Guo, H.; Ye, Y.; Sun, D.; Chen, Y.; Yang, T.; Zhang, J.; Ono, S.; Han, Z.; Zhang, Z. Electric-Field Control of Magnetism in a Few-Layered van der Waals Ferromagnetic Semiconductor. Nat. Nanotechnol. 2018, 13, 554–559.

[25] Miao, N.; Xu, B.; Zhu, L.; Zhou, J.; Sun, Z. 2D Intrinsic Ferromagnets from van der Waals Antiferromagnets. J. Am. Chem. Soc. 2018, 140, 2417–2420.

[26] Huang, C.; Feng, J.; Wu, F.; Ahmed, D.; Huang, B.; Xiang, H.; Deng, K.; Kan, E. Toward Intrinsic Toom-Temperature Ferromagnetism in Two-Dimensional Semiconductors. J. Am. Chem. Soc. 2018, 140, 11519–11525.

[27] Li, X.; Yang, J. Realizing Two-Dimensional Magnetic Semiconductors with Enhanced Curie Temperature by Antiaromatic Ring Based Organometallic Frameworks. J. Am. Chem. Soc. 2019, 141, 109–112.

[28] Fei, Z.; Huang, B.; Malinowski, P.; Wang, W.; Song, T.; Sanchez, J.; Yao, W.; Xiao, D.; Zhu, X.; May, A. F.; Wu, W.; Cobden, D. H.; Chu, J. H.; Xu, X. Two-Dimensional Itinerant Ferromagnetism in Atomically Thin Fe_3GeTe_2. Nat. Mater. 2018, 17, 778–782.

[29] Li, Q.; Yang, M.; Gong, C.; Chopdekar, R. V.; N'Diaye, A. T.; Turner, J.; Chen, G.; Schol, A.; Shafer, P.; Arenholz, E.; Schmid, A. K.; Wang, S.; Liu, K.; Gao, N.; Admasu, A. S.; Cheong, S.-W.; Hwang, C.; Li, J.; Wang, F.; Zhang, X.; Qiu, Z. Patterning-Induced Ferromagnetism of Fe_3GeTe_2 van der Waals Materials beyond Room Temperature. Nano Lett. 2018, 18, 5974–5980.

[30] Deng, Y.; Yu, Y.; Song, Y.; Zhang, J.; Wang, N. Z.; Sun, Z.; Yi, Y.; Wu, Y. Z.; Wu, S.; Zhu, J.; Wang, J.; Chen, X. H.; Zhang, Y. Gate-Tunable Room-Temperature Ferromagnetism in Two-Dimensional Fe_3GeTe_2. Nature 2018, 563, 94–99.

[31] Novoselov, K. S.; Castro Neto, A. H. Two-Dimensional Crystals-Based Heterostructures: Materials with Tailored Properties. Phys. Scripta. 2012, 146, 014006.

[32] Guinea, F.; Katsnelson, M. I.; Geim, A. K. Energy Gaps and a Zero-Field Quantum Hall Effect in Graphene by Strain Engineering. Nature Phys. 2010, 6, 30–33.

[33] Levy, N.; Burke, S. A.; Meaker, K. L.; Panlasigui, M.; Zettl, A.; Guinea, F.; Castro Neto, A. H.; Crommie, M. F. Strain-Induced Pseudo-Magnetic Fields Greater than 300 Tesla in Graphene Nanobubbles. Science 2010, 329, 544–547.

[34] Lloyd, D.; Liu, X.; Christopher, J. W.; Cantley, L.; Wadehra, A.; Kim, B. L.; Goldberg, B. B.; Swan, A. K.; Bunch, J. S. Band Gap Engineering with Ultralarge Biaxial Strains in Suspended Monolayer MoS_2. Nano Lett. 2016, 16, 5836–5841.

[35] Molle, A.; Goldberger, J.; Houssa, M.; Xu, Y.; Zhang, S. C.; Akinwande, D. Buckled Two-Dimensional Xene Sheets. Nat. Mater. 2017, 16, 163–169.

[36] Kou, L.; Tang, C.; Guo, W.; Chen, C. Tunable Magnetism in Strained Graphene with Topological Line Defect. ACS Nano. 2011, 5, 1012–1017.

[37] Ma, Y.; Dai, Y.; Guo, M.; Niu, C.; Yu, L.; Huang, B. Strain-Induced Magnetic Transitions in Half-Fluorinated Single Layers of BN, GaN and Graphene. Nanoscale 2011, 3, 2301.

[38] Zhou, Y.; Wang, Z.; Yang, P.; Zu, X.; Yang, L.; Sun, X.; Gao, F. Tensile Strain

Switched Ferromagnetism in Layered NbS_2 and $NbSe_2$. ACS Nano 2012, 6, 9727–9736.

[39] Ma, Y.; Dai, Y.; Guo, M.; Niu, C.; Zhu, Y.; Huang, B. Evidence of the Existence of Magnetism in Pristine VX_2 Monolayers (X = S, Se) and Their Strain-Induced Tunable Magnetic Properties. ACS Nano 2012, 6, 1695–1701.

[40] Kresse, G.; Furthmüller, J. Efficient Iterative Schemes for Ab Initio Total Energy Calculations Using a Plane-Wave Basis Set. Phys. Rev. B 1996, 54, 11169–11186.

[41] Kresse, G.; Furthmüller, J. Efficiency of Ab Initio Total Energy Calculations for Metals and Semiconductors Using a Plane-Wave Basis Set. Comput. Mater. Sci. 1996, 6, 15–50.

[42] Blöchl, P. E. Projector Augmented-Wave Method. Phys. Rev. B 1994, 50, 17953–17979.

[43] Kresse, G.; Joubert, D. From Ultrasoft Pseudopotentials to the Projector Augmented-Wave Method. Phys. Rev. B 1999, 59, 1758–1775.

[44] Perdew, J. P.; Zunger, A. Self-Interaction Correction to Density-Functional Approximations for Many-Electron Systems. Phys. Rev. B 1981, 23, 5048–5079.

[45] Zhuang, H. L.; Kent, P. R. C.; Hennig, R. G. Strong Anisotropy and Magnetostriction in the Two-Dimensional Stoner Ferromagnet Fe_3GeTe_2. Phys. Rev. B 2016, 93, 134407.

[46] Deiseroth, H. J.; Aleksandrov, K.; Reiner, C.; Kienle, L.; Kremer, R. K. Fe_3GeTe_2 and Ni_3GeTe_2—Two New Layered Transition-Metal Compounds: Crystal Structures, HRTEM Investigations, and Magnetic and Electrical Properties. Eur. J.

Inorg. Chem. 2006, 1561–1567.

[47] May, A. F.; Calder, S.; Cantoni, C.; Cao, H.; McGuire, M. A. Magnetic Structure and Phase Stability of the van der Waals Bonded Ferromagnet $Fe_{3-x}GeTe_2$. Phys. Rev. B 2016, 93, 014411.

[48] Chen, B.; Yang, J.; Wang, H.; Imai, M.; Ohta, H.; Michioka, C.; Yoshimura, K.; Fang, M. Magnetic Properties of Layered Itinerant Electron Ferromagnet Fe_3GeTe_2. J. Phys. Soc. Jpn. 2013, 82, 124711.

[49] Zhao, Y.; Gu, J.; Chen, Z. Oxygen Evolution Reaction on 2D Ferromagnetic Fe_3GeTe_2: Boosting the Reactivity by the Self-Reduction of Surface Hydroxyl. Adv. Funct. Mater. 2019, 29, 1904782.

[50] Dai, Z.; Liu, L.; Zhang, Z. Strain Engineering of 2D Materials: Issues and Opportunities at the Interface. Adv. Mater. 2019, 31, 1805417.

[51] Goodenough, J. B. Theory of the Role of Covalence in the Perovskite-type Manganites [La, M (II)] MoO_3. Phys. Rev. 1955, 100, 564–573.

[52] Kanamori, J. Crystal Distortion in Magnetic Compounds. J. Appl. Phys. 1960, 31, S14–S23.

[53] Anderson, P. W. New Approach to the Theory of Superexchange Interactions. Phys. Rev. 1959, 115, 2–13.